Electron Spin Relaxation in Ferromagnetic Insulators

R. C. FLETCHER, R. C. LeCRAW, AND E. G. SPENCER
Bell Telephone Laboratories, Murray Hill, New Jersey
(Received September 2, 1959)

A phenomenological description of electron spin relaxation in ferromagnetic insulators is developed using the rate of energy transfer between the uniform precession, the spin waves, and the lattice. This leads to an equation of motion containing T_{10}, the relaxation time of the uniform precession to the lattice; T_{2k}, the relaxation time of the uniform precession to the kth spin wave; and T_{1k}, the relaxation time of the kth spin wave to the lattice. Experimental measurements at 6200 Mc/sec are made on single crystal spheres of yttrium iron garnet to determine these times. In addition to measurements of resonance line width and high power saturation, these measurements include a frequency modulation method for measuring relaxation times. The theory provides an excellent fit to the experimental data over a range of surface roughness which varies the line width by a factor of 7.5. This enables the volume property, T_{1k}, to be determined experimentally in the presence of large surface scattering. The other volume property, T_{10}, is determined on the smoothest surface and is found to constitute the lower limit for reducing the line width in the present materials at room temperature. The theory and techniques described should facilitate a better understanding of the basic relaxation mechanisms.

I. INTRODUCTION

THE purpose of this paper is to obtain a phe-nomenonlogical description of the electron spin relaxation in ferromagnetic insulators and to present experimental data from which, using this description, fundamental relaxation parameters may be determined. In our description we will follow the general procedure of Bloembergen and Wang[1] by using the rate of transfer of energy between the main precession, the spin waves, and the lattice, but will modify their formulation in the light of the conceptions of Clogston et al.,[2] of coupling to spin waves by means of inhomogeneities in the magnetization, in a manner similar to that used by Callen.[3] We depart from the treatment of Bloembergen and Wang by treating each spin wave state separately, not necessarily in equilibrium with other spin wave states, nor with the uniform precession, nor with the lattice.

The experimental data were obtained on single crystal spheres of yttrium iron garnet (YIG) because of its high state of magnetic order and because the relaxation could be readily altered by varying the roughness of the surface.[4] Measurements were made of (1) the ferromagnetic resonance line width, (2) the critical rf magnetic field for saturation of the resonance, (3) the transverse relaxation time, and (4) the longi-tudinal relaxation time. The quantities (1)–(3) were obtained using modifications of existing techniques. Measurement of the longitudinal relaxation time, however, required the development of a rather refined modulation scheme in order to obtain sufficient sensi-tivity and accuracy.

II. DERIVATION OF EQUATIONS OF MOTION

To describe the relaxation of the magnetization it is convenient to consider the rate of transfer of energy as depicted in Fig. 1. Here, we divide up the total energy W into the amounts in each of the independent modes of the system. W_0 is the energy of the principal mode directly excited by the rf field while W_k is the energy of the kth spin mode. The term spin mode will be used for magnetostatic modes, influenced by sample shape, as well as for shorter wavelength modes, influenced by exchange forces. We use spin mode rather than spin wave to emphasize that we are dealing here with a normal mode of the system rather than just a component in the Fourier expansion of the magnetization. The former will contain a component of the magnetization along the magnetic field whose average is nonvanishing even for high order spin modes, while the latter does not.

The principle assumptions we will make are as follows: (1) We assume that the level of excitation of the spin system is low enough that the equations of motion can be linearized. The concept of describing the total motion of the system in terms of the super-position of spin modes is applicable only for such low levels of excitation. (2) We assume that the rf field couples to only one mode of the sample. For our experi-ments this mode will be the uniform precession. How-ever the resultant equations should be equally applicable to the direct excitation of magnetostatic spin modes by
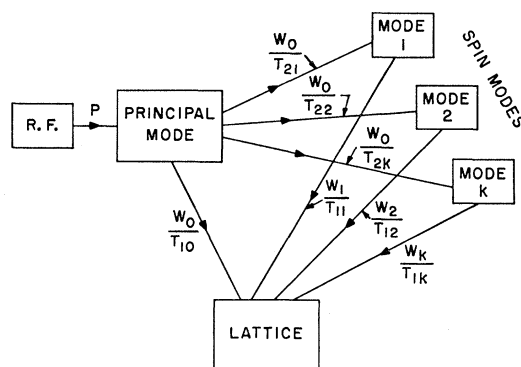

FIG. 1. Schematic diagram of the transfer of energy between the uniform precession, the spin modes, and the lattice.

[1] N. Bloembergen and S. Wang, Phys. Rev. **93**, 72 (1953).
[2] A. M. Clogston, H. Suhl, L. R. Walker, and P. W. Anderson, J. Phys. Chem. Solids **1**, 129 (1956).
[3] H. B. Callen, J. Phys. Chem. Solids **4**, 256 (1958).
[4] R. C. LeCraw, E. G. Spencer, and C. S. Porter, Phys. Rev. **110**, 1311 (1958).

nonuniform rf fields such as observed by White and Solt,[5] and by Dillon,[6] and by the type of spin wave "pinning" discussed by Kittel.[7] (3) We assume that the spin modes, once excited, do not react back on the principal mode. This back reaction is a second-order effect and becomes important only at high levels of excitation where saturation effects set it.

Consistent with the first assumption we can introduce characteristic coupling times. Thus T_{10} is the relaxation of the principal mode directly to the lattice, and T_{2k} is the coupling time from the principal mode to the kth spin mode. The subscripts one and two are used because of the close relation of these times to the T_1 and T_2 appearing in Bloch's equations describing paramagnetic relaxation.[8] Similarly the time T_{1k} is the net time for the kth spin mode to relax to the lattice. It may do this either by relaxing directly, or by coupling into other spin modes which can in turn relax to the lattice. If P is defined as the net power per unit volume absorbed by the sample, the energy transfer equations described by the above assumptions and definitions and depicted in Fig. 1 are given by

$$\frac{dW_0}{dt} = P - \frac{W_0}{T_{10}} - \sum_k \frac{W_0}{T_{2k}}, \quad (1)$$

$$\frac{dW_k}{dt} = \frac{W_0}{T_{2k}} - \frac{W_k}{T_{1k}}. \quad (2)$$

From these, the equation for the total energy,

$$W = W_0 + \sum_k W_k, \quad (3)$$

is given by

$$\frac{dW}{dt} = P - \frac{W_0}{T_{10}} - \sum_k \frac{W_k}{T_{1k}}. \quad (4)$$

Although these equations have exact solutions for many transient problems of interest (e.g., sinusoidal drive or free decay), further simplification results for the physical situations in which T_{1k} is reasonably constant for those spin waves which are excited (those with small T_{2k}). Under these circumstances, Eq. (4) reduces to

$$\frac{dW}{dt} = P - W_0 \left(\frac{1}{T_{10}} - \frac{1}{T_{1k}} \right) - \frac{W}{T_{1k}}. \quad (5)$$

In the remainder of the paper when T_{1k} appears without a $\sum_k$ before it, this implies that the above assumption has been used.

In order to relate these energy equations to the equations of motion of the magnetization, it is expeditious to make three additional assumptions: (4) We assume the principal mode, which is to be excited

directly, is the uniform precession. (5) We assume that the uniform precession couples to the spin waves by a process which conserves M_z and the total energy. This assumption will be valid for the type of coupling treated by Clogston et al.,[2] but will be invalid for the type of thermal scattering of spin waves considered by Kasuya.[9] This assumption can be shown to be equivalent to assuming only those spin modes are excited which have the same frequency as the main precession. (6) We assume the sample to be a spheroid so that $N_x = N_y$. This last assumption is necessary to be consistent with the fifth since otherwise M_z is not constant for the motion of the uniform precession.

The total energy is given by

$$W = (H - N_z M_s)(M_s - M_z) + \tfrac{1}{2} N_z (M_s - M_z)^2 + \tfrac{1}{2} N_x M_x^2 + \tfrac{1}{2} N_y M_y^2 + \sum_k (E_k + D_k), \quad (6)$$

where H is the dc magnetic field applied in the z-direction along the axis of revolution of the spheroid, M_s is the saturation magnetization, M_x, M_y, M_z are the components of the magnetization averaged over the sample, N_x, N_y, N_z are the demagnetizing factors, and E_k and D_k are the exchange and demagnetization energies, respectively, of the kth spin mode. The departure of M_z from its lowest energy value, M_s, we will call $-\Delta M_z$. This will be composed of the sum of all the longitudinal magnetizations, $-\Delta M_{zk}$, associated with the spin modes, together with the uniform precession, $-\Delta M_{z0}$:

$$\Delta M_z = M_s - M_z = \Delta M_{z0} + \sum_k \Delta M_{zk}. \quad (7)$$

The energy of the uniform precession is thus given by

$$W_0 = (H - N_z M_s)\Delta M_{z0} + \tfrac{1}{2} N_z (\Delta M_{z0})^2 + \tfrac{1}{2} N_x M_x^2 + \tfrac{1}{2} N_y M_y^2. \quad (8)$$

Since for each mode of the system the magnitude of the magnetization at each point is equal to M_s, we find for the uniform precession

$$(M_s - \Delta M_{z0})^2 + M_x^2 + M_y^2 = M_s^2, \quad (9)$$

which for small excitations reduces to

$$M_x^2 + M_y^2 = 2M_s \Delta M_{z0}. \quad (10)$$

With this relation, Eq. (8) can be written in either of the alternative forms

$$W_0 = [H + (N_T - N_z)M_s](M_x^2 + M_y^2)/2M_s, \quad (11)$$

or

$$W_0 = [H + (N_T - N_z)M_s]\Delta M_{z0}. \quad (12)$$

The part of ΔM_z associated with each spin mode, ΔM_{zk}, can be found from the requirement that M_z is conserved as main precession energy is converted to spin mode energy. Thus, consider in Eq. (6), that $E_k + D_k$ for a particular spin mode develop from a

[5] R. L. White and I. H. Solt, Phys. Rev. 104, 56 (1956).
[6] J. F. Dillon, Jr., Bull. Am. Phys. Soc. 1, 125 (1956).
[7] C. Kittel, Phys. Rev. 110, 1295 (1958).
[8] F. Bloch, Phys. Rev. 70, 460 (1946).

[9] T. Kasuya, Progr. Theoret. Phys. (Kyoto) 12, 802 (1954).

change in $M_x^2 + M_y^2$ keeping W and M_z constant:

$$E_k + D_k = -\tfrac{1}{2}N_T\delta(M_x^2 + M_y^2)$$
$$= -N_T M_s \delta \Delta M_{z0} = N_T M_s \Delta M_{zk}, \quad (13)$$

or

$$\Delta M_{zk} = (1/N_T M_s)(E_k + D_k). \quad (14)$$

Thus the total energy associated with the kth spin mode, i.e., the sum of magnetic, exchange, and demagnetizing energies, is

$$W_k = (H - N_z M_s)(\Delta M_{zk}) + E_k + D_k, \quad (15)$$

which with Eq. (13) reduces to

$$W_k = [H + (N_T - N_z)M_s](\Delta M_{zk}). \quad (16)$$

The total energy of the sample from Eqs. (12) and (16) is

$$W = [H + (N_T - N_z)M_s](M_s - M_z). \quad (17)$$

Thus we have an energy equation which does not explicitly contain spin mode parameters. Physically, this means that when energy is coupled from the main precession to the spin waves, transverse demagnetization energy due to $M_x^2 + M_y^2$ is converted into exchange energy and spin mode demagnetization energy. By expressing these latter as a particular fraction of the potential energy in the external field, we obtain an expression not involving E_k and D_k.

With the relations (11) and (17), the equations of motion (1) and (5) become

$$\frac{d}{dt}(M_x^2 + M_y^2) = \frac{2M_s P}{H + (N_T - N_z)M_s}$$
$$- (M_x^2 + M_y^2)\left(\frac{1}{T_{10}} + \sum_k \frac{1}{T_{2k}}\right), \quad (18)$$

$$\frac{d}{dt}(M_s - M_z) = \frac{P}{H + (N_T - N_z)M_s}$$
$$- \frac{M_x^2 + M_y^2}{2M_s}\left(\frac{1}{T_{10}} - \frac{1}{T_{1k}}\right) - \frac{M_s - M_z}{T_{1k}}. \quad (19)$$

In the absence of relaxation the torque equation is

$$\frac{d\mathbf{M}}{dt} = -\gamma(\mathbf{M} \times \mathbf{H}_e), \quad (20)$$

where H_e is the effective magnetic field at the sample and γ is the absolute value of the gyromagnetic ratio for electrons. Making this consistent with Eqs. (18) and (19) yields the basic equations of motion:

$$\frac{dM_{x,y}}{dt} = -\gamma(\mathbf{M} \times \mathbf{H}_e)_{x,y}$$
$$- \frac{M_{x,y}}{2}\left(\frac{1}{T_{10}} + \sum_k \frac{1}{T_{2k}}\right), \quad (21)$$

$$\frac{d(M_s - M_z)}{dt} = +\gamma(\mathbf{M} \times \mathbf{H}_e)_z - \frac{(M_x^2 + M_y^2)}{2M_s}$$
$$\times \left(\frac{1}{T_{10}} - \frac{1}{T_{1k}}\right) - \frac{(M_s - M_z)}{T_{1k}}. \quad (22)$$

Relation to Other Equations of Motion

(a) The Bloch Equations

The Bloch equations, introduced as a phenomenological description of paramagnetic relaxation, have been used also in ferromagnetic relaxation.[1] Equation (21) is exactly Bloch's equation for transverse relaxation providing that

$$\frac{1}{T_2} = \frac{1}{2}\left(\frac{1}{T_{10}} + \sum_k \frac{1}{T_{2k}}\right). \quad (23)$$

Equation (22) differs in general from the Bloch equation for longitudinal relaxation because of the presence of the second term on the right-hand side. In the event that $T_{10} = T_{1k}$, both our equations become identical with the Bloch equations.

It is interesting to note that even when T_{10} and T_{1k} are not equal, that the Bloch equations give a description of the motion of the system which has most of the essential features provided we find the appropriate expression for T_1. This expression is most easily found by examining the steady-state expression for the total energy, W^{ss}. From Eqs. (4) and (1),

$$W^{ss} = P\frac{1 + \sum_k (T_{1k}/T_{2k})}{(1/T_{10}) + \sum_k (1/T_{2k})}. \quad (24)$$

By equating this with the steady-state energy PT_1 given by the Bloch equations and using Eq. (23), we find that

$$T_1 = \frac{T_2}{2}\left(1 + \sum_k \frac{T_{1k}}{T_{2k}}\right). \quad (25)$$

When T_{1k} is constant and equal to T_{10} this expression reduces to $T_1 = T_{10}$ as was noted before. We have examined the time varying solutions of (21) and (22) for a sinusoidally varying P and for a free decay. For both these conditions the Bloch equations give a reasonable approximation using the relation (25) providing first, that T_{2k} has a minimum over which T_{1k} is relatively constant and second, that the condition

$$T_{10} \ll \sum_k (1/T_{2k}) \ll T_{1k} \quad (26)$$

does not apply. The latter condition is exceptional and probably not met in physical situations normally encountered.

It should be noted in Eq. (25) that in the absence of spin-spin coupling, T_2 increases to $2T_1$ and not to T_1 as has often been assumed. The factor of two is required

in order to conserve M. It is also interesting to note that $T_2 \approx 2T_1$ even in the presence of spin-spin coupling for the special case $\sum_k (T_{1k}/T_{2k}) \ll 1$. This is the condition in which the spin modes decay more rapidly than they are excited, which also conserves M.

(b) Callen's Dynamical Equation

A dynamical equation obtained from quantizing the spin waves into magnons and treating the problem quantum mechanically has been presented by Callen.[3] His equation is given in the form

$$d\mathbf{M}/dt = \alpha \mathbf{M} - \gamma(\mathbf{M} \times \mathbf{H}) - \lambda \mathbf{M} \times (\mathbf{M} \times \mathbf{H}) \quad (27)$$

where α, γ, and λ are complicated scalar functions of $\mathbf{M}$ and $\mathbf{H}$. Although the quantum mechanical approach used by Callen is different from the present paper, the underlying physical assumptions are the same. We would therefore expect to arrive at the same equation of motion. In his derivation, by using the magnon concept, Callen restricts the range of applicability to low levels of excitation in the same way as the present treatment. In this limit Callen's equation can be reduced to the form of Eqs. (21) and (22). It is believed that the energy balance approach in the present treatment has the advantages of conceptual clarity and simplicity which have led to an increased usefulness in interpreting experimental data.

(c) The Landau-Lifshitz Equation

The Landau-Lifshitz equation of motion[10] and its modification by Gilbert[11] have been used extensively to describe ferromagnetic relaxation. These both have the property of conserving the magnitude of the magnetization during relaxation. Experimental data will be presented on samples in which the spatially averaged magnetization is definitely not conserved. These equations would then be inapplicable. This is true even though microscopically the exchange forces keep adjacent spins very nearly aligned, so that locally the magnetization is conserved. Thus the Landau-Lifshitz equation may be a reasonable approximation on a microscopic scale, although inapplicable to the average magnetization.

III. THE MODULATION METHOD

The most difficult quantity to measure has been the relaxation of the component of magnetization along the magnetic field.[12] Our first efforts to measure this quantity were by a pulsed decay scheme similar to that

described by Bloembergen and Wang,[1] Damon,[13] and Farrar.[14] However, as the angle of opening of the uniform precession becomes smaller, as it must to avoid saturation effects in narrow line width materials, the signal due to the relaxation of the longitudinal magnetization decreases rapidly (as the square of the precession angle). The signal-to-noise ratio in the wideband detector used to detect pulse decay thus becomes prohibitively small in materials such as single crystal YIG. In order to obtain data in these materials a method for reducing the bandwidth is desirable. To achieve this a modulation scheme was devised.

The method consists of adjusting the applied dc magnetic field to resonance and sinusoidally modulating the microwave frequency at a low angular frequency Ω. We wish to examine the second harmonic components of the total energy W, proportional to the longitudinal magnetization [Eq. (17)], and W_0, proportional to $M_x^2 + M_y^2$ [Eq. (11)]. Let

$$(W_0)_{2\Omega} = A_0 \cos(2\Omega t), \quad (28)$$

$$(W)_{2\Omega} = A \cos(2\Omega t + \varphi). \quad (29)$$

By inserting these into Eqs. (1) and (5) and using the definition of T_2 in Eq. (23), we can eliminate P to find the ratio of amplitudes:

$$\left(\frac{A}{A_0}\right)^2 = \frac{[1 + (2T_{1k}/T_2) - (T_{1k}/T_{10})]^2 + (2\Omega T_{1k})^2}{1 + (2\Omega T_{1k})^2}. \quad (30)$$

When normalized in terms of their values at zero frequency, we obtain

$$\left[\frac{A(2\Omega)/A(0)}{A_0(2\Omega)/A_0(0)}\right]^2$$

$$= \frac{1 + (2\Omega T_{1k})^2 \left[\dfrac{T_2}{2T_{1k} + (1 - T_{1k}/T_{10})T_2}\right]^2}{1 + (2\Omega T_{1k})^2}. \quad (31)$$

The quantity in brackets on the left will be denoted by R. The numerator and denominator of R are the normalized amplitudes of the second harmonic components of ΔM_z and M_T^2, respectively. They are directly measurable. Since T_2 can be determined from the line width, the unknown quantities are T_{1k} and T_{10}. If $T_{10} = T_{1k}$, Eq. (31) has the simple form

$$R^2 = \frac{1 + (\Omega T_2)^2}{1 + (2\Omega T_{10})^2}, \quad (32)$$

where R approaches $T_2/2T_{10}$ for large Ω.

It is also useful to obtain an expression for $M_x^2 + M_y^2$ in terms of ΩT_2 for a frequency modulated rf field of constant amplitude. In this case the absorbed power P does not drop out. By an expansion of the driving

[10] L. Landau and E. Lifshitz, Physik. Z. Sowjetunion **8**, 153 (1935).

[11] T. A. Gilbert, Armour Research Institute (unpublished reports).

[12] Measurements of the relaxation of the transverse component by modulation techniques have been described previously, E. G. Spencer and R. C. LeCraw, Bull. Am. Phys. Soc. **3**, 145 (1958). See also J. I. Masters and R. W. Roberts, Jr., Suppl. J. Appl. Phys. **30**, 179S (1959).

[13] R. W. Damon, Revs. Modern Phys. **25**, 239 (1953).

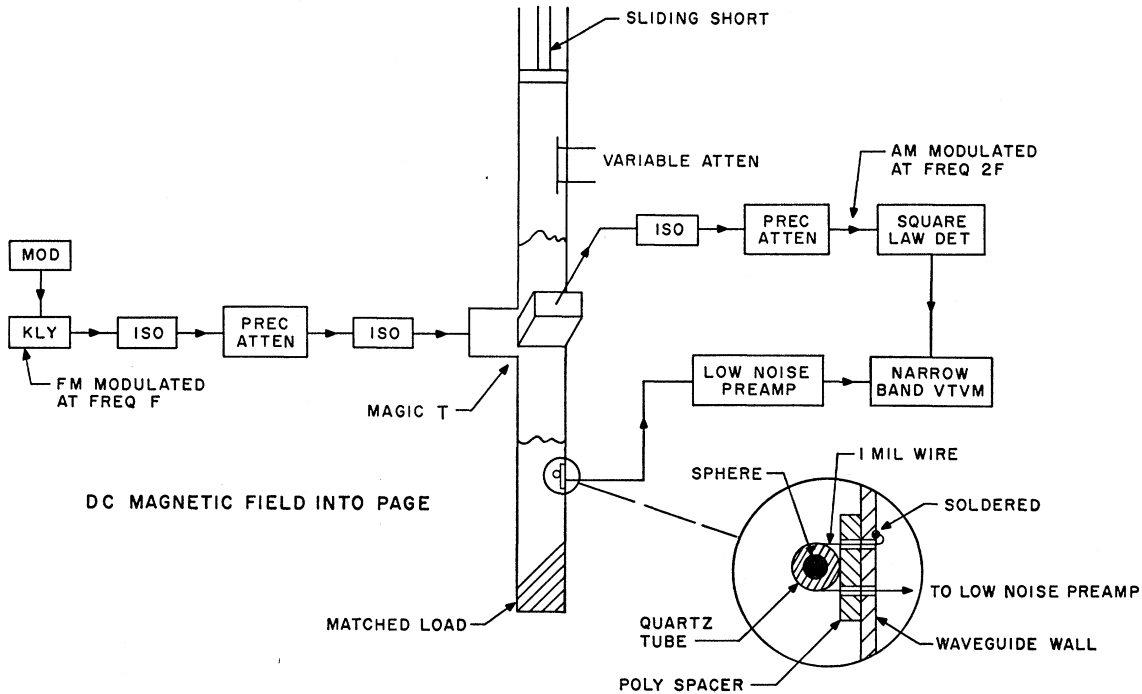[14] R. T. Farrar, J. Appl. Phys. **29**, 425 (1958).

FIG. 2. Schematic diagram of the experimental apparatus.

field in a Fourier series, in the limit of vanishingly small modulation amplitude $\Delta\omega$ (the peak frequency deviation), Eq. (21) yields the expansion for the second harmonic of $M_T{}^2 = M_x{}^2 + M_y{}^2$:

$$(M_T{}^2)_{2\Omega} = \frac{B}{\Omega^2}\left[\frac{1}{[1+(2\Omega T_2)^2]^{\frac{1}{2}}}\right.$$

$$\times \cos\left(2\Omega t - \sin^{-1}\frac{2\Omega T_2}{[1+(2\Omega T_2)^2]^{\frac{1}{2}}}\right) - \frac{1}{1+(\Omega T_2)^2}$$

$$\left.\times \cos\left(2\Omega t - 2\sin^{-1}\frac{\Omega T_2}{[1+(\Omega T_2)^2]^{\frac{1}{2}}}\right)\right], \quad (33)$$

where $B = 2M_s T_2(\Delta\omega)^2 P/H$. At vanishingly small modulation frequencies, Eq. (33) yields

$$(M_T{}^2)_{2\Omega=0} = -BT_2{}^2 \cos 2\Omega t. \quad (34)$$

The normalized ratio of amplitudes of $(M_T{}^2)_{2\Omega}$ from Eqs. (33) and (34) can be used in a modulation-type measurement of T_2 which should agree with T_2 as determined from line width measurements.

IV. EXPERIMENTAL PROCEDURE

The apparatus shown schematically in Fig. 2 is used for all measurements. A low Q klystron operating at a center frequency of 6200 Mc/sec is frequency modulated at a frequency $F = \Omega/2\pi$ by applying a sinusoidal voltage to the repeller. The frequency deviation of the klystron closely approximates a linear function of the

repeller voltage up to maximum frequency deviations as large as 10 Mc/sec. The maximum frequency deviation used for any of the data is 8.5 Mc/sec.

The klystron output is fed through isolators and a precision attenuator into the H-plane arm of a matched hybrid junction (magic T). Between the first isolator and precision attenuator there is a directional coupler for monitoring the power which is not shown in Fig. 2. Half the input power is incident on the sample, which is mounted on the narrow side wall of the waveguide, with about 0.08 in. of dielectric material between it and the wall. The other half is attenuated, phased properly, and reflected to null out the residual signal in the E-plane arm of the T when the dc field is off resonance and the klystron is unmodulated. Thus only the power reflected from the sample in the vicinity of the resonance line is detected, this being proportional to $M_T{}^2$.

When the dc field is on resonance and the klystron is frequency modulated at frequency F, the signal reflected from the sample and hence incident on the detector is amplitude modulated with its principal component at $2F$. The signal at the detector is of course also frequency modulated at frequency F. However, the crystal mount is broadband and sensitive only to the amplitude modulation.

The detector output is fed to a narrowband vacuum tube voltmeter (VTVM). The bandwidth of the VTVM for measurements of $M_T{}^2$ is 5 kc/sec at all modulation frequencies. The crystal is carefully selected and biased to be square law to within better than one percent, hence the detected signal is proportional to power or

M_T^2. From Eq. (11) it is seen that $W_0 \propto M_T^2$, hence the $2F$ component of M_T^2 is proportional to A_0. This component is measured as a function of $2F$, yielding the quantity $A_0(2\Omega)/A_0(0)$ in Eq. (31).

The quantity $A(2\Omega)/A(0)$ is obtained as follows: the spherical sample is wedged into a thin quartz tube with a wall thickness approximately six-tenths the radius of the sphere. The tube is then mounted on a small polystyrene slab 0.065 in. thick which in turn is mounted on the narrow side wall of the waveguide. The inside dimensions of the waveguide are 1.59×0.795 in. A one turn coil of one mil enameled wire is wound about the quartz tube with the plane of the coil perpendicular to the dc field, as shown in Fig. 2. One end of the coil is soldered to the waveguide and the other goes through a short piece of coaxial cable to a low noise preamplifier. The exact geometry of the coil is important and was experimentally optimized to produce minimum interaction with the sample as far as M_T is concerned and yet have sufficient pickup of ΔM_z. Excessive interaction with M_T results in broadening of the resonance line. The optimum diameter of the coil is about 1.6 times that of the sphere. The coil should be kept in the plane perpendicular to the dc field and should be centered about the equator of the sphere.

The design of the low noise preamplifier is also important. Two stages of wideband transformers are used before the first cathode follower tube to insure that the noise voltage of the resistance in the pickup coil circuit (~0.5 ohm) is dominant. Another wideband transformer is used between the cathode follower and the VTVM, again to insure that the noise of the input circuit containing the sample is dominant. The bandwidth of the VTVM for ΔM_z measurements is 500 cps from 0.1 Mc/sec to 1 Mc/sec, and 5 kc/sec above 1 Mc/sec. Since the ΔM_z signal has a factor which varies directly as the modulation frequency, the 500 cps bandwidth was unnecessary above 1 Mc/sec. The minimum signal-to-noise ratios were encountered at $2F = 0.1$ Mc/sec and were about 10 to 1. To obtain these good ratios, the peak deviations of the klystron from its center frequency were approximately $\gamma \Delta H$ in Mc/sec, the widest deviation being use for the widest

line width. The VTVM used was a selective microvoltmeter made by the Rhode and Schwarz Company, with bandwidth settings of 500 cps and 5 kc/sec.

From Eq. (17) it is seen that $W \propto \Delta M_z$, hence the $2F$ component of ΔM_z is proportional to A. This component is measured as a function of $2F$, yielding the quantity $A(2\Omega)/A(0)$ in Eq. (31).

The third directly measurable quantity, T_2, appearing in Eq. (31) is obtained as follows. It is well known that the line width ΔH between the points of half maximum absorption is related to T_2, as given in Eq. (23), by

$$\Delta H = 2/\gamma T_2. \qquad (35)$$

Assuming a circularly polarized applied rf field, it is easy to show that M_T^2, and hence the power reflected, varies with the dc field in the same manner as the absorbed power. It is worth noting here that although the rf field applied to the sample is linearly and not circularly polarized, it can be considered as the superposition of positive and negative circularly polarized fields, with the interaction of the negative circularly polarized field being negligible.

Thus T_2 is determined from the dc field between the points of half maximum reflected power, keepting the incident power constant. No frequency modulation is applied during the measurement. A number of points other than the half-maximum points were measured to check the line shape. It was found to fit Eq. (21), which is Lorentzian, very closely. To complete the relaxation measurements, T_2 was also obtained using the modulation scheme by fitting measured values of $(M_T^2)_{2\Omega}$ to Eq. (33).

The critical rf field H_{crit} for onset of saturation effects can also be measured with the apparatus shown in Fig. 2. The original form used to determine ΔH_k is given by[15]

$$H_{\text{crit}} = \Delta H (\Delta H_k / 4\pi M_s)^{\frac{1}{2}}, \qquad (36)$$

where ΔH_k is the "line width" of a z-directed spin wave, which we may write as $1/\gamma T_{1kz}$ to conform to our present nomenclature, and H_{crit} was presumed to be the value of rf field for the first observed decrease in χ''. Suhl recently has shown[16] that the presence of line

TABLE I. Surface treatment, diameter, line width and relaxation data on single crystal spheres of yttrium iron garnet at 6200 Mc/sec along the [111] axis. Surfaces 0-3 are for the same sample. Surface 4 is on a different sample from the same batch, measured to indicate the reproducibility of samples from the same batch. An estimated error on T_{10} is not given for surface 4 since complete curve fitting of the data to Eq. (31) was not done. The numbers in parentheses were determined for surface 3 and assumed to be independent of surface.

Surface Number	Surface treatment	Mean pit size (μ)	Diameter (Inch)	ΔH (oe)	From line width T_2 (mμsec)	From modulation			From $H_{\text{crit}} T_{1kz}$ (mμsec)
						T_2 (mμsec)	T_{1k} (mμsec)	T_{10} (mμsec)	
0	Linde A	0.3	0.036	0.44±0.01	258±5				
1	2/0 emory	10	0.032	3.56±0.05	32±0.5	31±1	102±2	(137)	(35)
2	4/0 emory	3	0.028	2.07±0.04	55±1	54±2	89±2	(137)	(35)
3	Linde A	0.3	0.027	0.47±0.01	242±5	242±5	137±5	137_{-5}^{+15}	35
4	Linde A	0.3	0.014	0.49±0.01	232±5	224±5	132	132	34

[15] H. Suhl, J. Phys. Chem. Solids 1, 209 (1957).
[16] H. Suhl, J. Appl. Phys. (to be published).

broadening due to inhomogeneity or impurity scattering alters the picture somewhat, and H_{crit} no longer coincides with the first observed decrease of χ''. It is necessary to curve fit the fall off of χ'' vs applied rf power to a set of curves for different ratios of intrinsic to scattered line width, and thus obtain a more correct value of H_{crit}. Only for an infinite ratio of intrinsic to scattered line width does H_{crit} in the new approach coincide with the point of first observed decrease in χ''.

A plot of χ'' vs applied power is obtained as follows. It has been pointed out previously that the absorbed power (proportional to χ'') varies as M_T^2, which is proportional to the power reflected from the sample. With the dc field on resonance and the modulation turned off, a reference level is set for the detector output. The two precision attenuators are then varied simultaneously in one db steps, with one decreasing and the other increasing in attenuation. (See Fig. 2.) Since the detector is accurately square law, its output at each pair of attenuator settings "plots" out χ'' vs the applied rf power. The absolute values of rf magnetic field in the waveguide are readily calculable. The two attenuators are of identical design and are calibrated both separately and against each other.

The effects of radiation damping on the observed line width and hence on T_2 should be considered in measurements on narrow line width materials.[17] For the size samples used, the effect is negligible for all but the most highly polished surface state. Here the error was only 4% (surface 3) and was determined experimentally by measuring the ratio of the reflected to incident power on resonance with no modulation. This ratio, when converted to fields, indicated a 4% reduction in the rf magnetic field applied to the sample
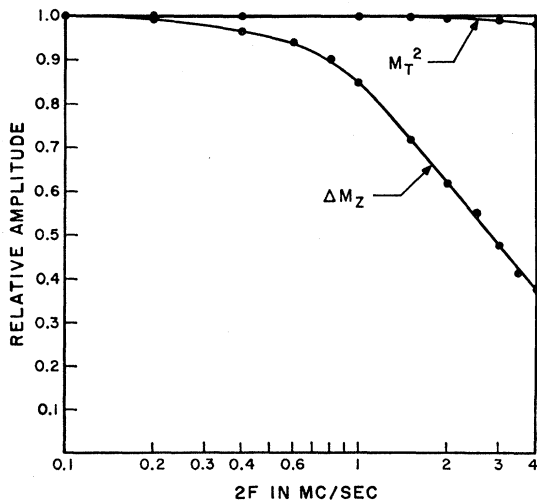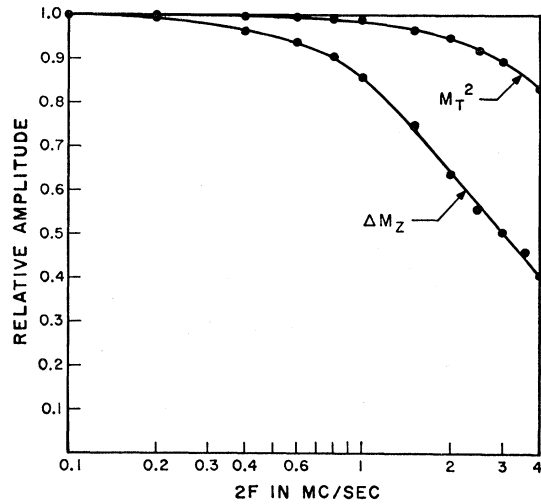

FIG. 4. Same measurements and sample as Fig. 3, for surface 2 with mean pit size of 3 microns.

compared with the incident field, and hence a corresponding error in line width. This correction has been applied to the data in Table I.

V. EXPERIMENTAL PROCEDURE

In order to obtain maximum correlation between data corresponding to different surface states, all measurements were made on the same sample of single crystal YIG (except for one additional sample from the same batch included to study sample reproducibility). Also it should be noted that for all data except H_{crit}, the applied rf field was maintained at least 3 db below the point of first evidence of saturation effects.

Initially the sample was ground and polished by the air-jet, tumbling technique to the smoothest polish available (Linde A) to be certain of the intrinsic

FIG. 3. The normalized second harmonic $(2F)$ components of ΔM_z and M_T^2, when the incident microwave power is frequency modulated at frequency F, for surface 1 with mean pit size of 10 microns.

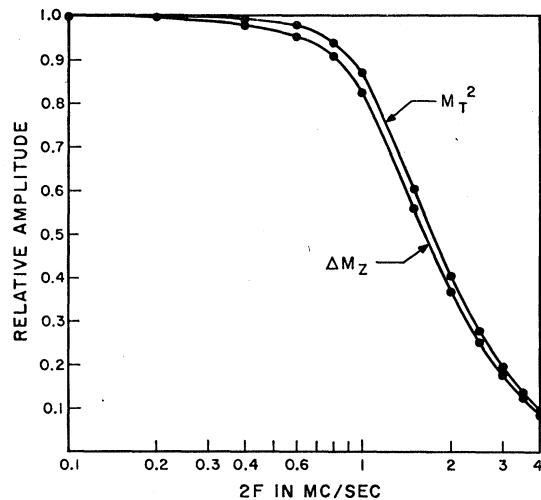[17] R. F. Trambarulo and E. H. Turner (private communication).

FIG. 5. Same measurements and sample as Fig. 3, for surface 3 with mean pit size of 0.3 micron.

quality. The line width was 0.44 oe at 6200 Mc/sec, at room temperature, and along the [111] axis (at which all subsequent measurements have been made). The sphere was then placed back in rougher grinders and ground successively to three different states of surface roughness as enumerated in Table I. The reduction in diameter at each stage was sufficient to make certain that the surface was covered uniformly with pits characteristic of the particular grit size.

After each grinding stage line width, relaxation, and saturation measurements were made. The line widths shown in Table I vary by about a factor of 7.5. The normalized amplitudes of the second harmonic ($2F$) components of ΔM_z and $M_T{}^2$ are shown as a function of $2F$ in Figs. 3, 4, and 5 for the successive surface conditions. For these curves the modulation amplitude (peak frequency deviation) was adjusted to approximately $\gamma\Delta H$ in Mc/sec. It is apparent from these curves that the character of the ΔM_z fall off is much different from $M_T{}^2$, particularly for the roughest surface (Fig. 3), demonstrating the inadequacy of a damping equation which conserves the average magnetization, such as the Landau-Lifshitz equation. As the polishing proceeds, it is seen that conservation of M is more nearly approached (Fig. 5).

Experimentally determined values of the quantity R^2 in Eq. (31), corresponding to Figs. 3–5, are plotted as the points in Fig. 6. Theoretical curves, calculated from Eq. (31), are shown by the solid curves in Fig. 6. The theoretical curves have used the value of T_2 determined from the line width, and values of T_{1k} and T_{10} to fit the points. A summary of these constants is
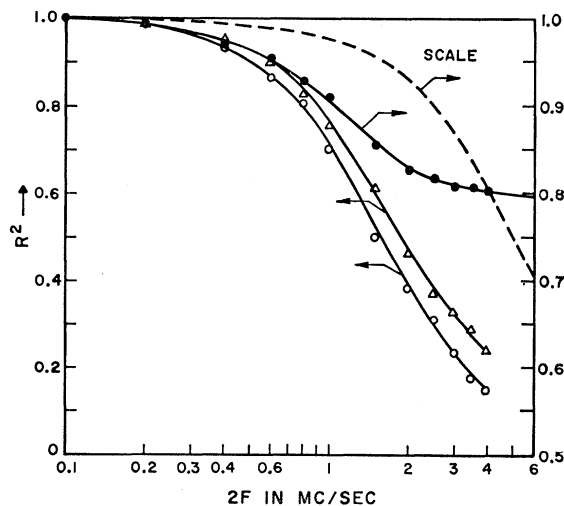
shown in Table I. For the two roughest surfaces, the theoretical curves are insensitive to the chosen value of T_{10} since most of the spin-lattice relaxation is occurring through the higher spin modes ($T_2 \ll 2T_{10}$). Thus to fit the point $R^2 = 0.24$ on surface 1, the value of T_{1k} varies only one percent as T_{10} varies from $T_{10} = T_{1k}$ to $T_{10} = \infty$.

For the smoothest surface, No. 3, however, the situation is different. The dashed curve in Fig. 6 is a theoretical curve calculated with the assumption that $T_{10} = \infty$, and T_{1k} adjusted to fit at the highest frequency point measured, 4 Mc/sec. A much superior fit is given for $T_{10} = T_{1k}$ shown by the uppermost solid curve. The accuracy indicated in Table I reflects the estimated departures which could be tolerated in the curve fitting. The value of T_{10} determined for surface 3 is assumed for the other surface states since T_{10} is presumably independent of surface roughness.
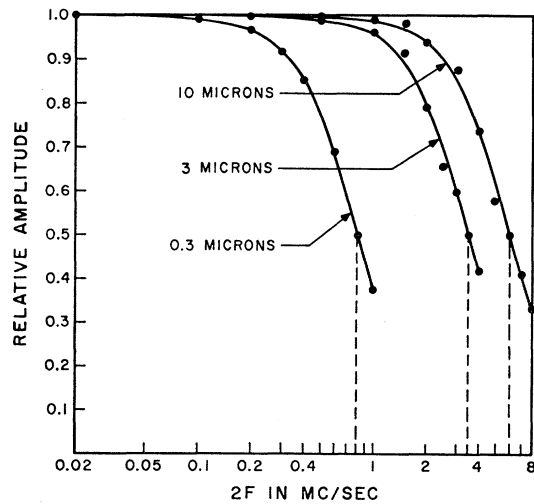

FIG. 7. Comparison of theory and experiment for the normalized second harmonic components of $M_T{}^2$ for small modulation amplitudes ($\sim 0.1\gamma\Delta H$ in Mc/sec) for surfaces 1–3, with mean pit sizes of 10, 3, and 0.3 microns, respectively. The solid curves are theoretical curves calculated from Eq. (33) and fitted at the one-half amplitude points.

FIG. 6. Comparison of theory and experiment for the square of the normalized ratio (R) of the second harmonic components of ΔM_z and $M_T{}^2$ for surfaces 1–3, with mean pit sizes of 10, 3, and 0.3 microns, respectively. The open circles are the experimental data on surface 1, the triangles are surface 2, and the solid circles are surface 3. The solid curves are theoretical curves calculated from Eq. (31). The dashed curve is Eq. (31) for surface 3, with T_{10} assumed to be infinite and T_{1k} adjusted to fit at 4 Mc/sec.

An additional check on the modulation method is provided by observation of the second harmonic component of $M_T{}^2$ at small modulation amplitudes ($\sim 0.1\gamma\Delta H$ Mc/sec). The measured, normalized amplitudes of $(M_T{}^2)_{2\Omega}$ are the points in Fig. 7. Theoretical curves calculated from Eq. (33) are shown by the solid curves. These contain one adjustable parameter, T_2, as listed in Table I. The good fit to the theoretical curves and the agreement with the line width determination of T_2 lend confidence to the modulation measurements.

Saturation measurements were made only for the most highly polished surface, No. 3, because of heating difficulties. The plot of χ'' vs applied rf power fits Suhl's theoretical curve[16] for $[T_{10} \sum (1/T_{2k})]^{-1} = 7$ and $H_{\mathrm{crit}} = 0.015$ oe for a reduction in χ'' of 15%. This gives

a ΔH_k of 1.65 oe or a relaxation time for the z-directed spin wave, T_{1kz}, of 35 mμsec.[18]

VI. DISCUSSION

The excellent fit of the theoretical curves to the experimental curves in Figs. 6 and 7 indicate the adequacy of the present description. For surfaces 1 and 2, the scattering of the uniform precession into spin modes is considerably greater than the "equivalent scattering" of the uniform precession due to T_{10}. If the assumption is made that the surface pits of surface 1 and 2 excite spin modes with wavelengths comparable to the pit size, a relatively unambiguous interpretation of T_{1k} is obtained for these two surfaces. For surface 3 the scattering into spin modes has been greatly reduced, so that only about 10% of the uniform precession energy relaxes to the lattice via the spin waves. Since this surface is so highly polished, it is likely that the small residual scattering is volume scattering caused by a small number of voids of the order of 25 microns known to be present in the sample. Thus the residual scattering for surface 3 is probably into modes with wavelengths greater than the surface pits of surfaces 1 and 2.

With this interpretation we see that T_{1k} varies comparatively slowly with surface roughness, but there is a trend for T_{1k} to decrease with decreasing wavelength. The points are shown in Fig. 8. The values of k for the two middle points were determined using the reciprocal of the mean pit size. The trend in T_{1k} with increasing k number is maintained in the determination of T_{1kz}, for a z-directed spin wave. However the T_{1kz} obtained by fitting Suhl's curves is probably too small. Suhl assumed that all of the inhomogeneity scattering into spin waves goes into the spin wave which is unstable at the lowest power. In addition he assumed that the nonlinear coupling term was independent of k. Further calculations by the authors indicate that these assumptions cause T_{1kz} in Table I to be approximately 25% low. The solid curve of Fig. 8 is drawn through the experimental points. However, it is possible that there is a minimum in the curve at $k=10\times10^4$ cm^{-1}, as would be predicted by an extension of the analysis of Kittel.[19] Because of the gap between the experimental points, the existence of such a minimum is not tested.

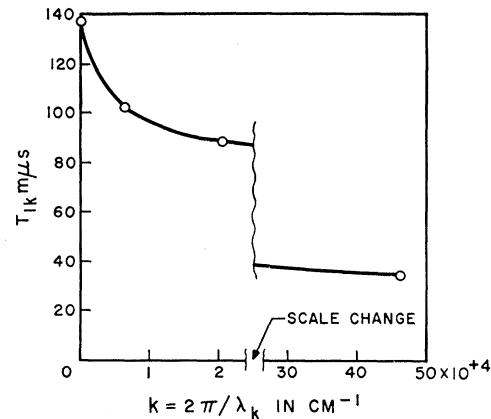It is worth noting that T_{1k} obtained even on the

FIG. 8. The spin-lattice relaxation time of spin waves of wave number k, vs. k. The point corresponding to surface 3 is not plotted for reasons explained in Sec. VI. The k scale is changed by a factor 10 at the point indicated.

roughest sample, represents information characteristic primarily of the bulk properties of the material. Thus T_{1k} obtained on a relatively unpolished sample is a considerably better indication of the intrinsic quality of the material than is ΔH or T_2, which depend strongly upon the surface. The value of T_{1k} and T_{10} measurements increases as the intrinsic line width of available materials becomes narrower, because of the increasing difficulty of obtaining a surface polish sufficiently fine to cause negligible line broadening.

VII. CONCLUSIONS

The successful combination of theory and experiment here indicates that this approach can be used to separate and evaluate the various surface and volume properties entering into the ferromagnetic relaxation process. Thus it should be possible to study the physical mechanisms giving rise to the bulk properties, T_{1k} and T_{10}, as a function of temperature, frequency, and rare earth[20] and other impurity content even though the line width still contains some broadening due to surface and volume imperfections.

[18] The ΔH_k of 1.65 oe obtained by curve fitting may be compared with the ΔH_k of 0.1 oe reported on YIG from the same batch, using the point of first observed decrease in χ'' to determine H_{crit}. R. C. LeCraw and E. G. Spencer, Suppl. J. Appl. Phys. 30, 185S (1959).
[19] C. Kittel, Phys. Rev. 110, 836 (1958).

[20] E. G. Spencer, R. C. LeCraw, and A. M. Clogston, Phys. Rev. Letters 3, 32 (1959).